SCIENCE CHINA
Information Sciences

• RESEARCH PAPER •

July 2017, Vol. 60 072202:1–072202:10
doi: 10.1007/s11432-016-0566-7

# Multi-objective optimal preliminary planning of multi-debris active removal mission in LEO

Yong LIU[1*], Jianan YANG[1], Yizhou WANG[1], Quan PAN[1] & Jianping YUAN[2]

[1]*School of Automation, Northwestern Polytechnical University, Xi'an* 710072*, China;*
[2]*School of Astronautics, Northwestern Polytechnical University, Xi'an* 710072 *, China*

Received July 9, 2016; accepted November 14, 2016; published online May 12, 2017

**Abstract** The goal of this paper is to develop a preliminary plan for a multi-nanosatellite active debris removal platform (MnADRP) for low-Earth-orbit (LEO) missions. A dynamic multi-objective traveling salesman problem (TSP) scheme is proposed in which three optimization objectives, i.e., the debris removal priority, the MnADRP orbital transfer energy, and the number of required nanosatellites are modeled respectively. A modified genetic algorithm (GA) is also proposed to solve the dynamic multi-objective TSP. Finally, numerical experiments involving partially real-world the debris data set are conducted to verify the efficacy of the proposed models and the solution method.

**Keywords** multi-debris active removal, optimal planning, multi-objective optimization, debris removal priority, genetic algorithm

**Citation** Liu Y, Yang J N, Wang Y Z, et al. Multi-objective optimal preliminary planning of multi-debris active removal mission in LEO. Sci China Inf Sci, 2017, 60(7): 072202, doi: 10.1007/s11432-016-0566-7

## 1 Introduction

Recent studies indicate that the debris population in the low Earth orbit (LEO) is growing at a dramatic rate, despite of current international debris mitigation policies [1]. Because of the high impact speed, debris items as small as 0.2 mm pose a realistic threat to human space activities and assets. To better preserve LEO resources, active debris removal (ADR) of massive upper stages and spacecraft fragments must be considered. Moreover, multiple items of debris should be removed in a single mission to reduce launch costs and shorten the overall spacecraft manufacture and preparation process [2].

An ADR mission typically involves rendezvous between a spacecraft and the debris targeted for removal. Hence, proximity operations, capturing, stabilization, and deorbiting maneuvers must be performed successfully. Recently, the multi-nanosatellite ADR platform (MnADRP) has been proposed [3], which consists of a mother spacecraft and a number of nanosatellites as its payloads. Under this scheme, the nanosatellites are released when the MnADRP is near the target debris, then perform the capturing and stabilization. Eventually, the mother spacecraft performs the main debris capturing, and the mother spacecraft and nanosatellites deorbit together with the debris into the Earth's atmosphere.

* Corresponding author (email: yong@nwpu.edu.cn)

 

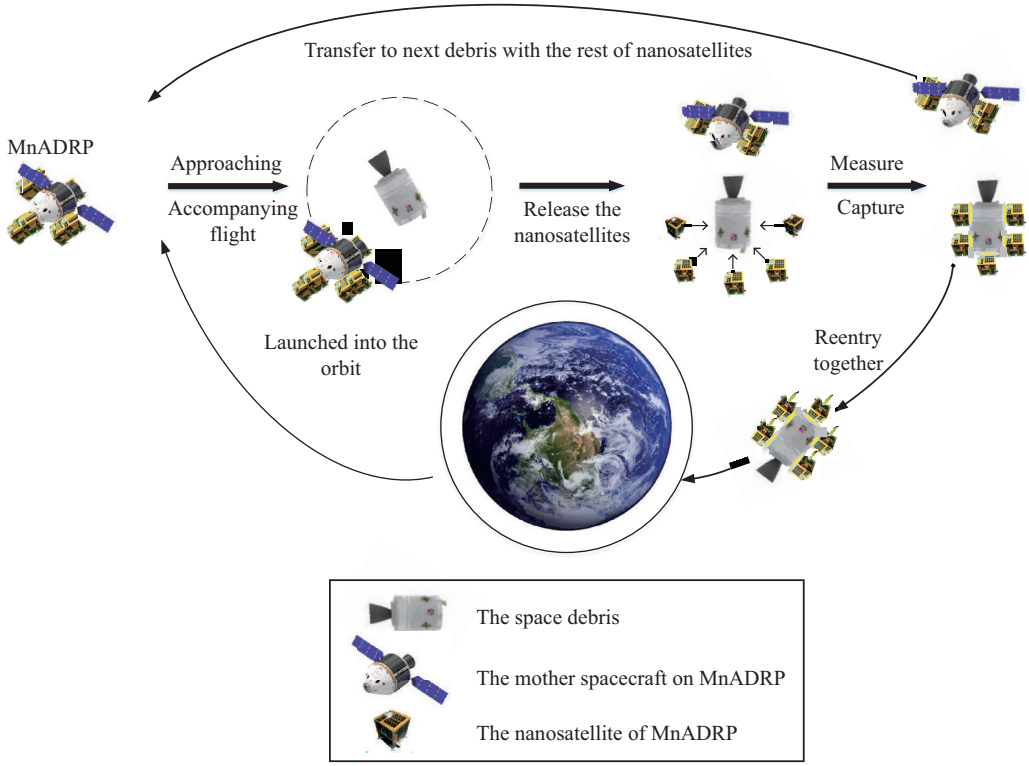


**Figure 1** Multiple space debris removal with MnADRP.

In this paper, the MnADRP is extended to facilitate the removal of multiple items of debris. The task flow is as follows. The MnADRP is launched into an initial orbit. After receiving the mission start command, it performs transfer, rendezvous and removal operations for a series of debris items, in accordance with a certain preliminary plan uploaded from the ground or embedded before its launch. In this plan the target debris, rendezvous sequence, and time-to-debris are specified, allowing the MnADRP to obtain high removal efficacy, subject to its payload, energy, and time budgets. When approaching each item of debris, the MnADRP mother spacecraft releases several nanosatellites, which can approach and capture the debris, eventually detumbling and deorbiting the debris. Then the MnADRP progresses to the next debris removal task, in according to the planned sequence. The entire mission process is shown in Figure 1. The factors rendering the MnADRP suitable for this mission are as follows. First, the mother spacecraft can transport sufficient energy for orbital transfer and nanosatellites for debris deorbiting. Second, the nanosatellite number and type can be adapted based on the size, mass, or motion of specific items of debris. Finally, following release from the mother spacecraft, nanosatellites can construct a network to conduct multi-source measurements of the debris, so as to enhance the precision of relative motion estimation. Moreover, the nanosatellites are low-cost because of the standardization and modulation of their systems.

The preliminary planning is a critical procedure for the multi-debris removal mission design, as it determines the target debris, the orbital transfer sequence, and the design requirements of the ADR spacecraft, such as its energy and the number of transported nanosatellites. This problem is first regarded as a single-objective optimization task. For example, in [4], the energy cost of an ADR spacecraft is optimized using a series method. In [5, 6], the debris removal sequence with the lowest energy cost is determined via brute force approach for four different scenarios. Moreover, in [7], this problem is solved under time and energy constraints for the three satellite debris clouds, Iridium 33, Cosmos 2251, and Fengyun 1C. Approaches to minimizing the energy cost for a chosen debris set, with consideration of the rendezvous time for each particular transfer strategy, are presented in [8, 9]. In recent years, multi-objective optimization has been introduced and has attracted considerable attention. For example, in [10], the mission duration and energy cost are taken as two optimization objectives under a Lambert

transfer strategy. Further, in [11], the same objectives are considered, but different deorbit scenarios are examined using the branch and bound approach. The total duration and energy cost are also utilized as optimization objectives in [12]; however, the time, energy, and nanosatellite budget are added as constraints.

This paper proposes a multi-objective optimization scheme and GA-based solution method for the preliminary planning of a multi-debris removal mission with an MnADRP, which maximizes the total debris removal priority while minimizing the orbital transfer energy and the number of nanosatellites required for debris removal. In the next section, the multi-objective optimization formulation and the energy-cost, nanosatellite-quantity cost, and debris priority models are elucidated. Then, the GA-based solving method is introduced. Finally, numerical experiments are conducted and the results are analyzed to verify the efficacy of the proposed method.

## 2 Problem formulation

### 2.1 TSP-based optimization formulation

In accordance with the mission procedure shown in Figure 1, in the preliminary planning stage of the multi-debris removal mission, all the data involved in the mission design can be modeled using the graph

$$\mathcal{G} = \{\boldsymbol{D}, \boldsymbol{V}(t), \boldsymbol{p}, \boldsymbol{m}\}, \tag{1}$$

where $\boldsymbol{D}$ denotes a set of vertices, where each vertex contains all the required parameters for each item of debris; $\boldsymbol{V}(t)$ is the time-dependent weighted connection matrix representing the orbital transfer cost for the MnADRP to move from one debris item to another; $\boldsymbol{p}$ is the vertex priority matrix representing the benefit when each debris item is removed; and $\boldsymbol{m}$ is the vertex cost matrix representing the number of nanosatellites expended on each debris item to accomplish the deorbit operation.

If the MnADRP is regarded as a moving node on $\mathcal{G}$, the preliminary planning problem then becomes the problem determining the optimal path on this graph. For multi-debris removal, the primary aim is the removal of the most dangerous items of debris while generating minimal mission cost (including the energy and nanosatellite-quantity costs). Therefore, a multi-objective optimization scheme can be adopted to solve this problem, the details of which are as follows:

$$\underset{\left(\begin{array}{cccc} d_1 & d_2 & \cdots & d_n \end{array}\right), \left(\begin{array}{cccc} t_1 & t_2 & \cdots & t_n \end{array}\right)}{F} \left( \min \sum_{i=1}^{n} \Delta v_i \ \min \sum_{i=1}^{n} m_i \ \max \sum_{i=1}^{n} P_i \right) \tag{2}$$

$$\text{s.t.} \begin{cases} \left\{ \begin{array}{cccc} d_1 & d_2 & \cdots & d_n \end{array} \right\} \subseteq \left\{ \begin{array}{cccc} D_1 & D_2 & \cdots & D_N \end{array} \right\}, \\ 0 \leqslant t_1 \leqslant t_2 \leqslant \cdots \leqslant t_n \leqslant T_{\max}, \\ \sum_{i=1}^{n} m_i(d_i) \leqslant m_{\max}, \\ \sum_{i=1}^{n} \Delta v_i \leqslant \Delta v_{\max}, \end{cases}$$

where the debris set $\mathrm{D} = \{D_1, D_2, \ldots, D_N\}$ contains the total number of debris items $N$ requiring removal, and each debris item $D_j$ is modeled by $\left(a_{D_j}, e_{D_j 0}, I_{D_j}, \Omega_{D_j}, \omega_{D_j}, M_{D_j 0}, m_{D_j}, B_{D_j}, P_{D_j}, A_{D_j}^{MR}, R_{D_j}^{CS}\right)$ $(j \in \{1, 2, \ldots, N\})$, where $a_{D_j}$ is the orbit altitude, $e_{D_j}$ is the eccentricity, $I_{D_j}$ is the orbit inclination, $\Omega_{D_j}$ is the right ascension of ascending node (RAAN), $\omega_{D_j}$ is the argument of perigee, $M_{D_j 0}$ is the mean anomaly at epoch, $m_{D_j}$ is the dry mass, $B_{D_j}$ is the normalized drag term, $P_{D_j}^{C}$ is the collision probability, $A_{D_j}^{MR}$ is the area to mass ratio, $R_{D_j}^{CS}$ is the radar cross section (rcs), all of $D_j$. Suppose that $n\,(n < N)$ debris items are chosen for removal and take $d_i$ as the $i$th debris item to be removed $(i \in \{1, 2, \ldots, n\})$. Further, $\Delta v_i \in \boldsymbol{V}(t)$ is the cost of orbital transfer to $d_i$ at time $t_i$, measured by the required velocity change (note that the spacecraft mass is not included in this preliminary planning as it can eventually be determined

from the velocity change), $m_i \in \boldsymbol{m}$ is the number of nanosatellites required for removal of $d_i$, and $P_i \in \boldsymbol{p}$ is the removal priority of $d_i$. The $P_i$, $\Delta v_i$, and $m_i$ models are elucidated in the next three subsections, respectively; these models detail the dynamics and decision strategies. The total mission-time, energy-cost, and nanosatellite budgets are labeled $T_{\max}$, $\Delta v_{\max}$, and $m_{\max}$, respectively. The debris removal sequence is $\{d_1, d_2, \ldots, d_n\}$ and its corresponding time sequence is $\{t_1, t_2, \ldots, t_n\}$.

Before examination of the multi-objective optimization, we must confirm that these objectives are coupled. As an increasing number of debris items are removed during a given mission, the overall priority $\sum_{i=1}^{n} P_i$ is summed, however, the transfer energy cost $\sum_{i=1}^{n} \Delta v_i$ and the number of nanosatellites $\sum_{i=1}^{n} m_i$ also continue to increase. Thus, these three objectives are coupled. When $n$ is fixed, the coupling mainly lies in collecting $n$ debris items such that the maximal debris priority summation value is obtained. However, this is typically achieved without realization of the minimal transfer cost or minimal nanosatellite quantity cost. That is a tradeoff exists between these factors.

### 2.2 Debris removal priority model

The debris removal priority $P_i$ is the factor indicating the threat level of a certain debris item $d_i$. It also reflects the gain from the removal of that debris item. However, the debris threat levels vary according to different missions. For example, with regard to space environment protection, removal of the most dangerous debris items in a given environment is the main objective. However, for the protection of a single spacecraft, the debris posing the greatest threat to this orbit of that particular spacecraft should be removed first. Therefore, the selection of debris for removal depends on each mission task, and the ranking regime is set by the specific mission requirements. Examination of the ranking method is not the purpose of this paper, but inclusion of a ranking scheme is essential based on the problem definition, so the following scheme is a general version application to any debris set.

Typically, a simplified ranking regime is proposed focusing on the most significant debris parameters relevant to the space environment of concern. According to [13, 14], besides the orbital parameters, the debris mass, size, shape, ballistic coefficient term, area-to-mass ratio, rcs and material properties can be recorded for consideration in this scheme. In addition, some software program indicate the collision risk of each debris item. Here, we take the examples given in [2, 4, 5, 7] and analyze their potential risk to the space environment. Then the debris characteristics of collision probability $P^C$, mass $m$, area-to-mass ratio $A^{MR}$, and rcs $R^{CS}$ are utilized to construct the ranking scheme. In general, debris items having higher $m$, $R^{CS}$, and $A^{MR}$ produce a greater number of debris item after collision, and $P^C_{d_j}$ directly reflects the threat of $d_i$ to the space environment.

Using the simple multiple-attribute decision-making (MADM) method, a weighted normalized summation is used to represent the debris $P_i$. The ranking scheme used to optimize the $P_i$ levels is

$$P_i = \omega_1 \times N^i_P + \omega_2 \times N^i_{\text{mass}} + \omega_3 \times N^i_{\text{AMR}} + \omega_4 \times N^i_{\text{rcs}}, \tag{3}$$

where $N^i_P$, $N^i_{\text{mass}}$, $N^i_{\text{AMR}}$, $N^i_{\text{rcs}}$ are the normalized collision probability, the normalized mass, the normalized area-to-mass ratio, and the normalized rcs of $d_i$ respectively, and $\omega_1$, $\omega_2$, $\omega_3$, $\omega_4$ are the respective weights of these attributes, satisfying $\omega_1 + \omega_2 + \omega_3 + \omega_4 = 1$. The normalization is performed using the full range of these parameters in a single debris set, to redefine each parameter with a value from 0 to 1.

### 2.3 Transfer energy cost model

In the MnADRP scenario, the transfer strategy is used to complete the orbital maneuvers, specifying the details of the optimization model and the experiment conducted in this study. Thus, the transfer strategy is the method used to alter each orbital parameter. Based on recent research, the method using the perturbing force of the Earth's equatorial bulge is very efficient [8]. This bulge is modeled by the $J_2$ zonal term and causes precession of the orbit plane (the node of the plane to be detailed). This transfer strategy was first applied to ADR by Cerf [15], and can dramatically reduce the energy cost $\Delta v$. However, this approach is passive and the mission duration is uncontrollable because, after each removal process, the ADR spacecraft must wait until it meets the next debris item with identical RAAN. To

manage the tradeoff between the mission duration and energy cost, Cerf proposed a drift orbit that uses the natural precession of the Earth to change the RAAN [15]. The drift orbit is an intermediate circular orbit between two debris orbits, which can adapt the RAAN variation rate to the debris-rendezvous time sequence. The drift-orbit altitude $a$ and inclination $I$ are determined by the nonlinear optimization of $\Delta v$, which ensures that each drift orbit exhibits the lowest energy consumption while completing the RAAN adjustment.

The propulsion type is another important aspect of the transfer strategy. Chemical propulsion is direct but has higher energy consumption that the alternative Electronic propulsion facilitates a steady acceleration, but it is more complex [8, 16]. For this preliminary planning of the multi-debris removal operation, it is reasonable to assume that the MnADRP employs chemical propulsion.

Therefore, in this article, the following transfer strategy is utilized to change the orbit parameters:

- $I$ is achieved via a velocity change at the orbit node.
- $a$ is achieved via Hohmann transfer. Here,

$$\begin{cases} \Delta v = \sqrt{\dfrac{\mu}{r_1}} \cdot \left( \sqrt{\dfrac{2r_2}{r_1 + r_2}} - 1 \right), \\ \Delta v' = \sqrt{\dfrac{\mu}{r_2}} \cdot \left( -\sqrt{\dfrac{2r_1}{r_1 + r_2}} + 1 \right), \end{cases} \tag{4}$$

where $\mu$ is the standard gravitational parameter, $r_1$ and $r_2$ are the radii of the initial and destination orbits, respectively, and $\Delta v$ and $\Delta v'$ are the two velocity changes induced by the Hohmann transfer.

- The RAAN $\dot{\Omega}$, which incorporates the $J_2$ zonal term of the Earth's equatorial bulge perturbing force, is obtained, with

$$\dot{\Omega} = -\frac{3}{2} J_2 \sqrt{\mu} R_T^2 (a + R_T)^{-\frac{7}{2}} \cos I, \tag{5}$$

where $J_2 = 1.08266 \times 10^{-3}$ is the first zonal term, $R_T = 6378137\,\mathrm{m}$ is the Earth's equatorial radius, $a$ is the orbital radius for circular orbits only, $I$ is the inclination. The unit of the RAAN change is rad/s.

- Mean motion $M$ is obtained. The difference in the $M$ values of two objects is determined by the the difference in their orbital periods. However, compared with the drift-orbit transfer duration, the time required for the phase maneuver can be ignored, as this operation has a duration of only several revolutions.
- The eccentricity $e$ is obtained. In LEO, the majority of the orbits are near-circular. Therefore, in this article, all the orbits are regarded as circular to facilitate a simple calculation.
- Argument of periapsis $\omega$: The periapsis arguments are the same as those for circular orbits.

Here the $I$ and $a$ maneuvers are completed together, as in the study by Cerf [8]. However, the propulsion with the smaller initial velocity in the Hohmann transfer is chosen as most appropriate. Therefore, in this transfer strategy, all the energy cost is determined by the velocity change, i.e., $\Delta v$ which is determined by the change of $I$ and $a$. The adjustment of the other orbital elements does not consume any energy, because a circular orbit and natural perturbing force are employed. The reduced energy consumption obtained by a longer transfer duration is the main advantage of this transfer strategy.

Because the drift-orbit transfer strategy presented here is similar to that employed by Cerf [8], nonlinear optimization is still employed to determine $\Delta v$. The cost matrix is constructed by considering the rendezvous time and transfer duration separately, thereby determining the required rapidity of the drift-orbit RAAN change. This RAAN change rate is dependent on the drift orbit, as indicated by (5), and determined by the orbit $I$ and $a$. When the MnADRP must move to the debris item for removal, it must move to the current debris orbit to derft orbit, before transferring from the drift orbit to the next debris orbit. Therefore, the $\Delta v$ differ for different drift orbits. Hence, the redundancy of the RAAN change rate requires nonlinear programming of the drift-orbit $I$ and $a$, with the aim of selecting the drift orbit with the lowest $\Delta v$.

Meanwhile the Response Surface Method (RSM) is a rapid means of determining the energy cost, i.e. $\Delta v$. (this method has also been used by Cerf [8]. This cost matrix performs well with bilinear

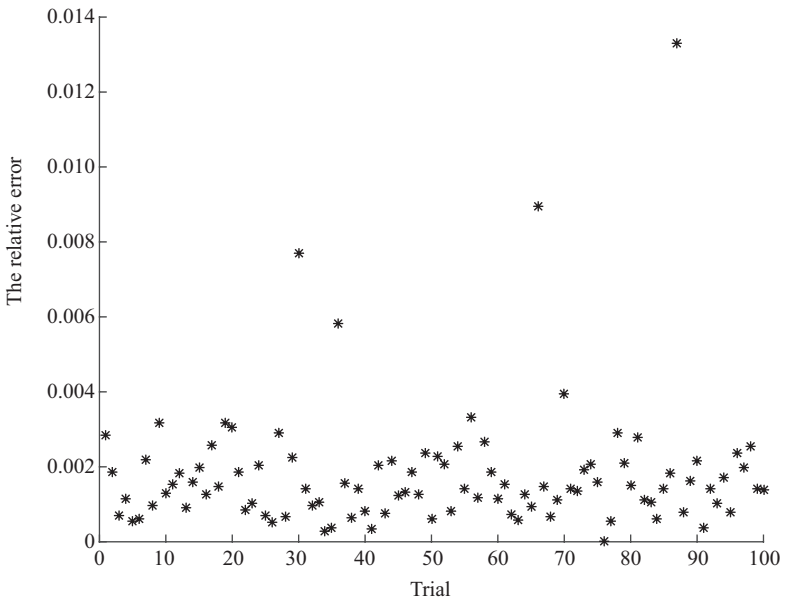


**Figure 2** Relative error caused by RSM.

interpolation, and the relative error caused by the RSM is shown in Figure 2. The cost matrix indexes correspond to a discrete rendezvous time and transfer duration, and the surface between them is regarded as linear. Thus, the cost between its four vicinity indexes can be calculated via bilinear interpolation.

### 2.4 Nanosatellites quantity cost model

In this scenario the MnADRP performs orbital transfer and nanosatellite release only, whereas the deorbit operation is one of the tasks completed by the nanosatellites. It is assumed that these nanosatellites carry same propulsion kits to facilitate debris reentry following their attachment to the target debris. Ideal nanosatellite constellation performance corresponds to zero energy waste during debris deorbiting. Therefore, using the rocket equation [17], we propose that the number of nanosatellites $m_i$ required for the removal of each debris item can be determined from

$$(m_i - 1) \cdot f_{\Delta v} \leqslant m_{d_i} \cdot \left(1 - \mathrm{e}^{-\frac{\Delta v_i^{\mathrm{d}}}{v_e}}\right) \leqslant m_i \cdot f_{\Delta v}, \tag{6}$$

$$m_i = \left\lceil \frac{m_{d_i}}{f_{\Delta v}} \cdot \left(1 - \mathrm{e}^{-\frac{\Delta v_i^{\mathrm{d}}}{v_e}}\right) \right\rceil, \tag{7}$$

where $m_{d_i}$ is the mass of $d_i$, $v_e$ is the effective exhaust velocity, $f_{\Delta v}$ is the fuel mass of the nanosatellites (it is assumed that the nanosatellite mass correspond to its fuel mass), and $\Delta v_i^{\mathrm{d}}$ is the velocity change needed to deorbit $d_i$ (corresponding to a transfer to a 100-km-altitude reentry orbit).

It is certain that the nanosatellites released in order to deorbit the debris must provide sufficient orbital transfer ability, but this should not be excessive. Therefore, given that $m_i$ is an integer, this value, which correspond the total provided fuel mass, should be more than the required fuel mass. Further, one less nanosatellite will not complete the deorbit as Eq. (6). Note that in the rocket equation, the initial mass is assumed to be $m_{d_i}$, while the final mass is derived from the initial mass subtracting the mass of nanosatellites attached to the debris.

## 3 GA-based solution method

As regards the preliminary design of the multi-debris removal mission, the mission plan must be decided prior to launch, and the optimization must first be conducted on the ground. Thus, almost all methods capable of TSP problem solution can be tailord to this dynamic optimization scheme. In previous

research on ADR missions, the branch and bound algorithm [15], simulated annealing [8], the ant colony approach [18], the brute force approach [16], the series method [4], the inver-over algorithm [7], and the genetic algorithm (GA) [19] have all been used for optimization.

The GA has the benefit of global search, and its mutation step is more likely to prevent local optima. Thus, this approach is suitable for the dynamic TSP model considered in this study, if the removal time can be encoded into the solution space. Therefore, in this article, the code and decode method is modified and a multi-debris-removal modified GA is proposed.

### 3.1 Genetic algorithm design

The basic concept of the GA remains unchanged. That is, the initial-generation population is determined, and selection, crossover, and mutation are employed to evolve this generation. The evolution is terminated once fitness convergence or the maximal evolution time is attained. However, for the present problem the state vector differs from the GA parameter optimization, being that defined in (8). It is assumed that, once the MnADRP arrives at a target debris item, it completes the nanosatellite-release operation within a single day. Therefore, if the time resolution corresponds to 1 d, the debris rendezvous time is identical to the time at which the MnADRP departed the previous debris site. Therefore, the time sequence is a set of integers from 1 to 365, representing the rendezvous time, and the total mission duration is 1 year. The solution space $x$ is represented as follows:

$$x = \begin{pmatrix} d_1 & \cdots & d_n \\ t_1 & \cdots & t_n \end{pmatrix}, \quad \text{s.t.} \begin{cases} \left\{ d_1 \ \cdots \ d_n \right\} \subset \left\{ D_1 \ \cdots \ D_N \right\}, \\ t_1 < \cdots < t_n. \end{cases} \tag{8}$$

Therefore, the feasible solution region can be regarded as being comprised of these two variants:

- The debris sequence simulated by the permutation of $n$ integers from $N$ (the total number of elements in the debris set);
- The rendezvous time sequence simulated by the ordered combination of $n$ integers from 365 rendezvous times (a 1-year total mission duration with 1-day accuracy).

### 3.2 Fitness function design

The fitness function is determined by the optimization objectives of the GA. This function is a scalar variant representing the fitness of an individual solution for a task, and a higher fitness level corresponds to a higher probability of natural selection. However, in the multiple-objectives case, the fitness of an individual solution is not determined by a single objective. In [20], the benefit- and cost- type objectives are employed as the fitness-function numerator, and denominator, respectively. The costs and benefits are normalized to the 0 to 1 range, so as accommodate the unit difference. Hence, in this article, the multiple objectives are transferred to a single objective in the form of a fitness function using (9), where $\text{normalized}(\cdot)$ is the normalization operator (the scale of each objective is detailed in the subsequent experiment), $\omega_P$, $\omega_v$, and $\omega_m$ are the weights of the normalized $\sum_{i=1}^{n} P_i$, the normalized $\sum_{i=1}^{n} \Delta v_i$, and the normalized $\sum_{i=1}^{n} m_i$.

$$\begin{aligned} &F\left( \min \sum_{i=1}^{n} \Delta v_i \ \min \sum_{i=1}^{n} m_i \ \max \sum_{i=1}^{n} P_i \right) \\ &= \max \left( \frac{\omega_P \times \text{normalized}\left(\sum_{i=1}^{n} P_i\right)}{\omega_v \times \text{normalized}\left(\sum_{i=1}^{n} \Delta v_i\right) \times \omega_m \times \text{normalized}\left(\sum_{i=1}^{n} m_i\right)} \right). \end{aligned} \tag{9}$$

As for the constraints, implementing these restricts in the selection step is similar to filtering the solution of each trial after the optimization. However, the latter approach is easier and the solution is not bounding to a local optimum. Therefore, in this paper, the constraints were implemented after the optimization, being employed as a filter to discount the solution out-of-boundary that.

**Table 1** Debris set

| No. | Alt.(km) | Inc.(°) | RAAN (°) | Mass (kg) | AMR ($m^2$/kg) | Collision probability | RCS ($m^2$) |
|---|---|---|---|---|---|---|---|
| 1 | 700 | 97 | 0 | 12 | 3 | 0.013 | 0.6756 |
| 2 | 710 | 97.3 | 90 | 12 | 2 | 0.014 | 2.5000 |
| 3 | 720 | 97.6 | 180 | 12 | 4 | 0.015 | 0.2201 |
| 4 | 730 | 97.9 | 270 | 12 | 5 | 0.016 | 4.5029 |
| 5 | 740 | 98.2 | 18 | 12 | 6 | 0.017 | 0.0710 |
| 6 | 750 | 98.5 | 108 | 12 | 7 | 0.018 | 0.0372 |
| 7 | 760 | 98.8 | 198 | 35 | 8 | 0.019 | 0.0563 |
| 8 | 770 | 97.1 | 288 | 77 | 9 | 0.020 | 0.0410 |
| 9 | 780 | 97.4 | 36 | 110 | 10 | 0.021 | 0.0606 |
| 10 | 790 | 97.7 | 126 | 48 | 11 | 0.022 | 0.3181 |
| 11 | 800 | 98 | 216 | 10 | 12 | 0.023 | 2.9784 |
| 12 | 810 | 98.3 | 306 | 12 | 13 | 0.024 | 0.1259 |
| 13 | 820 | 98.6 | 54 | 12 | 14 | 0.025 | 0.0579 |
| 14 | 830 | 98.9 | 144 | 12 | 15 | 0.026 | 0.0550 |
| 15 | 840 | 97.2 | 234 | 22 | 7 | 0.027 | 0.0363 |
| 16 | 850 | 97.5 | 324 | 53 | 8 | 0.028 | 0.0523 |
| 17 | 860 | 97.8 | 72 | 170 | 9 | 0.029 | 0.2321 |
| 18 | 870 | 98.1 | 162 | 50 | 10 | 0.030 | 0.0538 |
| 19 | 880 | 98.4 | 252 | 35 | 11 | 0.031 | 0.0414 |
| 20 | 890 | 98.7 | 342 | 48 | 12 | 0.032 | 0.0745 |
| 21 | 900 | 99 | 360 | 7 | 13 | 0.033 | 0.1090 |

## 4 Experiment and results

The optimization model is applied in experiment in order to test the solution. The RSM method utilized by Cerf [8] is used to calculate the energy costs $\Delta v_i$, and it is assumed that the nanosatellites are identical to each other and carry deorbit kits with some chemical propulsion.

### 4.1 Scenario settings

The debris set in [8], which was created to test the optimization method presented in that study, is comprised of a set of LEO debris items with uniformly distributed RAAN. In the present study, other parameters necessary to rank the $d_i$ based on their $P_i$ and to determine $m_i$ are added to the debris set. Thus, further data elements are created in this study, based on the satellite catalog (SATCAT), the union of concerned scientists (UCS) satellite database, the two-line element (TLE) sets data from space-track, and studies researching the collision probability [21] and area-to-mass ratio [22]. This resultant data set is comprised of partially realistic parameters as shown in Table 1, where "Alt" represents the orbit altitude of debris, "Inc" represents the orbit inclination of debris. It is adequate for testing of the algorithm and optimization model.

As in [2], the specific impulse $I_{sp}$ is set to 300 s, which is the average exhaust speed, and the nanosatellite mass is taken as 10 kg. The weight of each parameter in the priority ranking is 0.25, and the normalizing scale of each parameter is from its minimum to its maximum.

Based on the possible results for the three objectives ($\sum_{i=1}^{n} P_i$, $\sum_{i=1}^{n} \Delta v_i$, and $\sum_{i=1}^{n} m_i$), all the weights of the components in the fitness function are set to 1, the $\Delta v_i$ normalization scale is 0 to 120000 m/s, the $m_i$ normalization scale is 5 to 47, and the $P_i$ normalization scale is 0.1261 to 0.4140.

With regard to this GA optimization method, the maximum generation $NG_{\max}$ is set to 6000, the population of each generation $NP$ is 100, the probability of crossover $Pc$ is 0.9, and the probability of mutation $Pm$ is 0.02. The termination condition is the mean of the population's fitness function, and is 0.999 times the maximum fitness function.

We conducted 100 trials, and a trial with 1000 generation required a processing time of approximately 80 s on an Intel Core i7 processor computer.

**Table 2** Best individuals solutions according to each objective

| Gene. | Debris Seq. | Time Seq. | Fitness Fun. | RSM cost | $\sum_{i=1}^{n} m_i$ | $\sum_{i=1}^{n} P_i$ |
|---|---|---|---|---|---|---|
| 958 | 11-4-21-2-13 | 23-107-246-339-355 | **407.3899** | 3088.42 | **8** | 0.3417 |
| 1857 | 3-11-15-7-19 | 3-163-171-234-361 | 169.0654 | **1076.72** | 14 | 0.2197 |
| 501 | 21-2-14-11-4 | 38-124-224-300-364 | 269.8589 | 4700.93 | **8** | 0.3435 |
| 682 | 2-11-19-4-12 | 1-129-191-239-362 | 181.5300 | 3522.46 | 11 | **0.3453** |

**Table 3** Best individual solutions corresponding to each objective under constraints

| Gene. | Debris Seq. | Time Seq. | Fitness Fun. | RSM cost | $\sum m_i$ | $\sum p_i$ |
|---|---|---|---|---|---|---|
| 336 | 11-15-4-21-5 | 19-93-167-311-361 | **264.2767** | 2776.47 | **9** | 0.2938 |
| 1857 | 3-11-15-7-19 | 3-163-171-234-361 | 169.0654 | **1076.72** | 14 | 0.2197 |
| 149 | 2-7-11-19-4 | 29-126-166-256-347 | 159.4608 | 2963.87 | 13 | **0.3421** |

### 4.2 Results analysis

The best individual solution yielded by each trial was selected based on the highest fitness function in the final generation. (The details of this process are not included here, because of the paper length restriction.) For the best individuals solution determined from the 100 trials, each objective was evaluated. The most fit individual solutions are listed in Table 2, where $\sum_{i=1}^{n} m_i$ represents the overall nanosatellite cost, and $\sum_{i=1}^{n} P_i$ is the debris priority summation. The individual solution with the optimal fitness evolved in 958 generations, as the three objectives are all competitive. The lowest- $\sum_{i=1}^{n} \Delta v_i$ individual solution evolved in 1857 generations, with an RSM cost of only 1076.72 m/s. Again, $\sum_{i=1}^{n} m_i$ is an integer, and 40 solutions spend eight nanosatellites. Based on the other two objectives, two comparatively good individuals were chosen from these 40 solution, as they exhibited the lowest $\sum_{i=1}^{n} \Delta v_i$ or removed the debris with the highest $\sum_{i=1}^{n} P_i$ in the eight-nanosatellite cost band. The result with the highest $\sum_{i=1}^{n} P_i$ among the 100 trials is given in the final row of Table 2, where "Gene." represents the number of generations of the solution, "Debris Seq." represents the removal debris sequence, "Time Seq." represents the removal time sequence, "Fitness Fun." represents the fitness function value of each solution.

After the optimization, the true cost of the final solution for each trial was calculated, using the same nonlinear programming as used to construct the cost matrix. Figure 2 shows the relative error between the energy cost calculated using RSM and using nonlinear programming. Each point was calculated by using

$$E_r = \frac{\sum_{i=1}^{n} \Delta v_i^{\mathrm{RSM}} - \sum_{i=1}^{n} \Delta v_i^{np}}{\sum_{i=1}^{n} \Delta v_i^{np}}, \tag{10}$$

where $E_r$ is the relative error of the most fit individual solution in each trial, and $\Delta v_i^{\mathrm{RSM}}$ and $\Delta v_i^{np}$ are the costs of orbital transfer to $d_i$ at $t_i$ determined by RSM and nonlinear programming, respectively.

According to the above results, the majority of relative errors have values of approximately 0.2%, with some of them are even less than 0.1%; this indicates that the error caused by the RSM is sufficiently low for optimization. Therefore, the use of RSM to boost the process is appropriate.

As there are constraints to consider, the mission budgets employed here are 3-km/s chemical propulsion, and a maximum of 20 nanosatellites. Among the 100 trials, 18 trials satisfy these constraints. From these solutions, Table 3 shows the best individuals solutions according to the three objectives and the constraints.

The individual with the lowest $\sum_{i=1}^{n} \Delta v_i$ survived after the filter had been applied, whereas those with best fitness function and the highest $\sum_{i=1}^{n} P_i$ did not. However the new, most-fit individual solution under constraints corresponds to the individual solution with the lowest $\sum_{i=1}^{n} m_i$. Further, the iteration for the highest-priority individual solution terminated after only 149 generations, indicating that this objective can be matured easily.

The solution given by this multi-objective optimization model is more reasonable than other existing models and, after 100 trials one individual solution with the best historic performance can be identified; these results indicate that this method is suitable for the optimization model considered in this work.

Note that other studies of multi-debris removal missions, have not considered debris prioritization during the optimization, or the algorithms they employed are not adapted to the features of this time-variant TSP problem. Finally, the application of filtering to the unconstrained solution and the RSM method both work well in boosting the process.

## 5 Conclusion

A multi-objective optimization framework for preliminary planning of an MnADRP for a multi-LEO-debris removal mission is proposed. A model incorporating debris removal prioritization with debris-specific parameters is constructed and incorporated into the optimization formulation, together with energy and nanosatellite-payload cost models. A modified GA algorithm is introduced to solve the optimization problem. Numerical experiments conducted on partially real-world debris data confirm the efficacy of the proposed method. Future work may include investigations of online planning for an MnADRP in the context of mission recovery owing to unexpected mission failures, along with transfer orbit design refinement for an MnADRP for multi-debris removal based on the preliminary plan.

**Acknowledgements** This work was supported by National Science Foundation of China (Grant Nos. 61503304, 61374162), Fundamental Research Funds for the Central Universities (Grant No. 3102015ZY048).

**Conflict of interest** The authors declare that they have no conflict of interest.

### References

1 Liou J C. Engineering and technology challenges for active debris removal. Progr Propul Phys, 2013, 4: 735–748
2 Braun V, Lüpken A, Flegel S, et al. Active debris removal of multiple priority targets. Adv Space Res, 2013, 51: 1638–1648
3 Bogdan U, Nayak M. A cooperative multi-satellite mission for controlled active debris removal from low Earth orbit. In: Proceedings of the Aerospace Conference, Big Sky, 2015. 1–15
4 Barbee B W, Alfano S, Pinon E, et al. Design of spacecraft missions to remove multiple orbital debris objects. In: Proceedings of the Aerospace Conference, Big Sky, 2011. 1–14
5 Liou J C. An active debris removal parametric study for LEO environment remediation. Adva Space Res, 2011, 47: 1865–1876
6 Liou J C, Johnson N L. Instability of the present LEO satellite populations. Adv Space Res, 2008, 41: 1046–1053
7 Izzo D, Getzner I, Hennes D, et al. Evolving solutions to TSP variants for active space debris removal. In: Proceedings of the Annual Conference on Genetic and Evolutionary Computation, Madrid, 2015. 1207–1214
8 Cerf M. Multiple space debris collecting mission: optimal mission planning. J Optimiz Theory App, 2015, 167: 195–218
9 Yu J, Chen X Q, Chen L H. Optimal planning of LEO active debris removal based on hybrid optimal control theory. Adv Space Res, 2015, 55: 2628–2640
10 Madakat D, Morio J, Vanderpooten D. Biobjective planning of an active debris removal mission. Acta Astronaut, 2013, 84: 182–188
11 Bérend N, Olive X. Bi-objective optimization of a multiple-target active debris removal mission. Acta Astronaut, 2016, 122: 324-335
12 Jing Y, Chen X Q, Chen L H. Biobjective planning of GEO debris removal mission with multiple servicing spacecrafts. Acta Astronautica, 2014, 105: 311-320
13 Nations U. Technical Report on Space Debris. 1999
14 Mehrholz D, Leushacke L, Flury W, et al. Detecting, tracking and imaging space debris. ESA Bull, 2002, 40: 128–134
15 Cerf M. Multiple space debris collecting mission-debris selection and trajectory optimization. J Optimiz Theory App, 2013, 156: 761–796
16 Martin T, Pérot E, Desjean M C, et al. Active debris removal mission design in low Earth orbit. Progr Propul Phys, 2013, 4: 763–788
17 Chobotov V A. Orbital Mechanics. 2nd ed. Oxford: Oxford University Press, 2002. 87–115
18 Stuart J, Howell K, Wilson R. Application of multi-agent coordination methods to the design of space debris mitigation tours. Adv Space Res, 2015, 57: 1680–1697
19 Hokamoto S. Genetic-algorithm-based rendezvous trajectory design for multiple active debris removal. In: Proceedings of the International Symposium on Space Technology and Science, Okinawa, 2011
20 Li C M. Optimization Method. 1st ed. Nanjing: Southeast University Press, 2009
21 Braun V, Lüpken A, Flegel S, et al. Active debris removal of multiple priority targets. Adv Space Res, 2013, 51: 1638–1648
22 Thomas S. Properties of the high area-to-mass ratio space debris population at high altitudes. Adv Space Res, 2008, 41: 1039–1045